Open Ceramics 14 (2023) 100369

Contents lists available at ScienceDirect

Open Ceramics

journal homepage: www.sciencedirect.com/journal/open-ceramics

Determination of cohesion and friction angle of a MgO-C refractory at room and elevated temperatures

Maximilian Klopf [a,*], Dietmar Gruber [b]

[a] K1-MET GmbH, 8700, Leoben, Austria
[b] Montanuniversitaet Leoben, Chair of Ceramics, 8700, Leoben, Austria

ARTICLE INFO

Handling Editor: Dr P Colombo

Keywords:
Cohesion
Friction angle
MgO–C refractory

ABSTRACT

The use of constitutive models in thermomechanical finite element modelling of refractory linings requires knowing the temperature-dependent material parameters. The mechanical testing of carbon-containing refractory materials at elevated temperatures necessitates the protection of samples from oxidation. Therefore, the test concept of the modified shear test (MST) was further developed and a setup was designed to protect the carbon-containing materials from oxidation. A carbon-containing magnesia refractory (MgO–C), which is usually applied in secondary metallurgy for steel ladle refractory linings, was selected as the material of interest. The setup allows the determination of cohesion and friction angle of MgO–C refractories under reducing conditions at temperatures up to 1500 °C. The procedure allows a material parameters determination from uniaxial loading. While coked and as-delivered samples showed different behaviours, a significantly higher cohesion was noted in the as-delivered material. The results showed that the cohesion is highly temperature-dependent, whereas the friction angle remains nearly unaffected.

1. Introduction

In industrial applications, the primary causes of mechanical loads in refractory linings are thermal expansion and temperature gradients [1]. Finite Element (FE) simulation is an effective tool for utilizing various constitutive models for the determination of in-service stress states [2–4]. The simulated stress paths show that multiaxial compressive stresses, shear stresses and tensile stresses are developed in the refractory linings. It is essential to test the material behaviour under these loading conditions to determine the parameters of the constitutive models. Temperature-dependent material parameters of resin bonded carbon-containing refractories are available for creep and mode I fracture [5,6]. The Drucker-Prager yield criterion [7], which describes the shear strength in dependence of the hydrostatic pressure, requires the experimental determination of two material parameters: cohesion d and friction angle β. Standardised testing methods such as triaxial compression tests [8] or direct shear tests [9], are limited to room temperature or slightly elevated temperatures due to the setup. However, supplying material data up to maximum application temperature, allows to predict the refractory behaviour in service. A modified shear test (MST) [10] was developed using two sample geometries to determine the cohesion and friction angle of refractory materials under uniaxial loading at elevated temperatures. In this study, the existing testing setup was modified, allowing the cohesion and friction angle of carbon-containing refractories to be determined up to the application temperature.

2. Material and testing method

A commercially available resin-bonded MgO–C brick was selected as the material of interest in this study, which is typically used as a steel ladle slag zone lining in secondary metallurgy. The refractory was mainly composed of fused magnesia, sintered large crystal magnesia and graphite, with a residual carbon content of 10% after coking. The refractory exhibited a CaO/SiO_2 ratio (C/S-ratio) of 2.16. The C/S ratio is a key factor in characterising a product's refractoriness [11]. The material properties and oxide compositions are summarised in Table 1.

The MgO–C refractory was tested in two different states: as-delivered (DS) without pre-treatment and coked state (CS). For the CS sample, it was subjected to coking prior to the test. In this study, coking refers to a heat treatment at 1000 °C for 5 h under reducing conditions (in a coke bed) to pyrolyze the resin. The coked MgO–C material was composed of

* Corresponding author.
E-mail address: maximilian.klopf@k1-met.com (M. Klopf).

https://doi.org/10.1016/j.oceram.2023.100369
Received 21 March 2023; Accepted 9 May 2023
Available online 9 May 2023

Table 1
Oxide composition and selected material properties of the resin-bonded MgO–C refractory (Standards: chemical analysis EN ISO 12677 and physical properties according to EN 993-1).

	MgO [%]	Al_2O_3 [%]	Fe_2O_3 [%]	CaO [%]	SiO_2 [%]	C [%]	Density [g/cm^3]	Porosity [vol%]
MgO–C	97.1	0.2	0.6	1.3	0.6	10	3.07	4

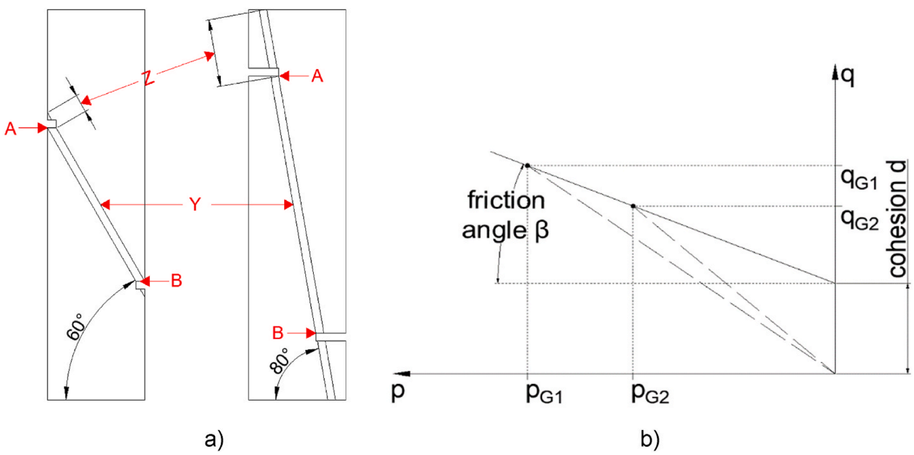

Fig. 1. a) Geometry G1 (60°-notch, left) and geometry G2 (80°-notch, right), b) schematic *p-q* diagram.

Table 2
Calculation factors for *p* and *q* for geometry G1 and G2 in MPa/kN.

	fp [MPa/kN]	*fq* [MPa/kN]
G1, 60°-notch	−2.672	0.803
G2, 80°-notch	−3.123	0.807

MgO grains and fines, graphite flakes and pyrolytic carbon [12–14].

Various testing methods [8,9,15] are available to determine the cohesion and friction angle of soils and hard rocks. However, they are limited to relatively low temperatures. In this study, MST was employed as the testing method, which was developed earlier by Dahlem et al. [10]. The MST is applicable for refractory materials to obtain the friction angle and cohesion up to application temperatures by uniaxial loading. The linear Drucker-Prager criterion [7] was applied throughout the evaluation (eqs. (1)–(3)).

$$q = -p \cdot \tan(\beta) + d \tag{1}$$

$$\text{with } p = -\frac{1}{3} \cdot (\sigma_1 + \sigma_2 + \sigma_3) \tag{2}$$

$$\text{and } q = \sqrt{\sigma_1^2 + \sigma_2^2 + \sigma_3^2 - \sigma_1\sigma_2 - \sigma_1\sigma_3 - \sigma_2\sigma_3} \tag{3}$$

where q is the von Mises stress, p is the hydrostatic pressure and $\sigma_{1,2,3}$ denote the principal stresses.

For the evaluation in the *p-q* diagram, two sample geometries with different inclined notch angles are required to get the two necessary failure points (Fig. 1). The dimensions of the MST samples were 37.5·37.5·150 mm^3. Angles of 60° (geometry G1) and 80° (geometry G2) were used for the inclination of the notches. As shown previously [10], G1 and G2 fulfil the requirement of shear failure in the ligament area for various refractories. The inclined notch Y depths of G1 and G2 are 7.5 and 8.5 mm, respectively. Z is the distance between the horizontal notch and edge of the sample, which are 7.5 and 26 mm for G1 and G2, respectively. In all cases, the notch width is 3 mm.

The maximum uniaxial loads of three samples for each geometry were averaged and converted into von Mises stress (q) and hydrostatic

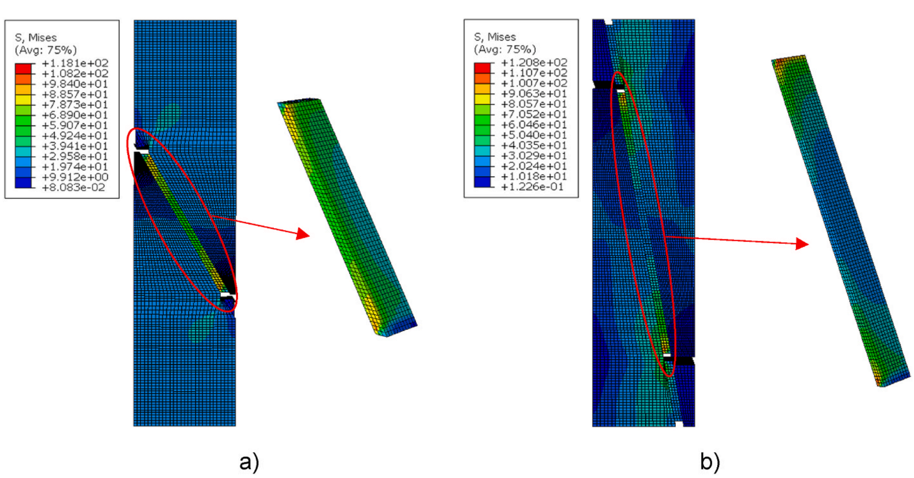

Fig. 2. Distribution of von Mises stress q in geometry a) G1 and b) G2.

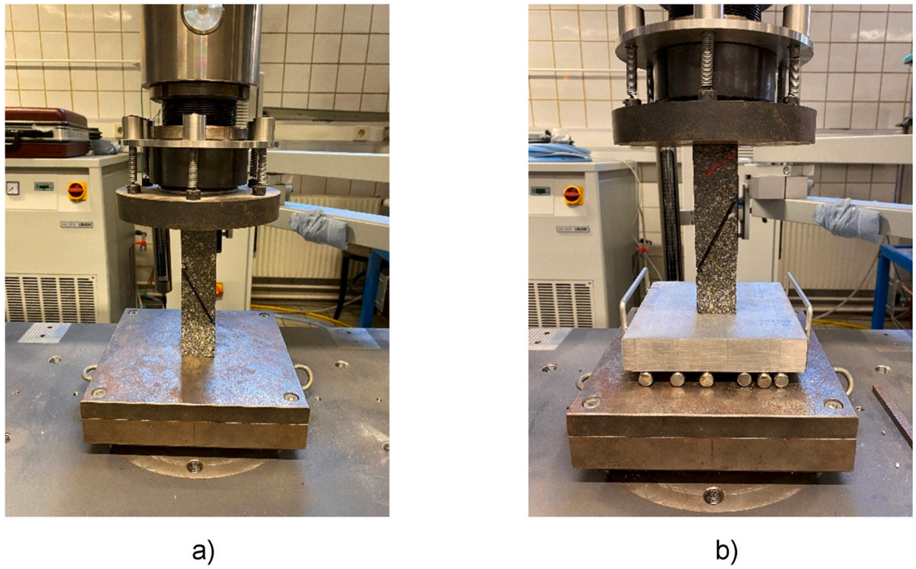

Fig. 3. a) Setup without plate and b) Setup with rollers and supporting plate beneath the MST sample at room temperature.

Table 3
Average maximum force of samples with and without rollers and supporting plate.

	without plate		with plate	
	60°-notch samples	80°-notch samples	60°-notch samples	80°-notch samples
	force [kN]	force [kN]	force [kN]	force [kN]
MW	24.50	22.66	24.39	20.28
SD	1.28	0.43	1.88	0.56

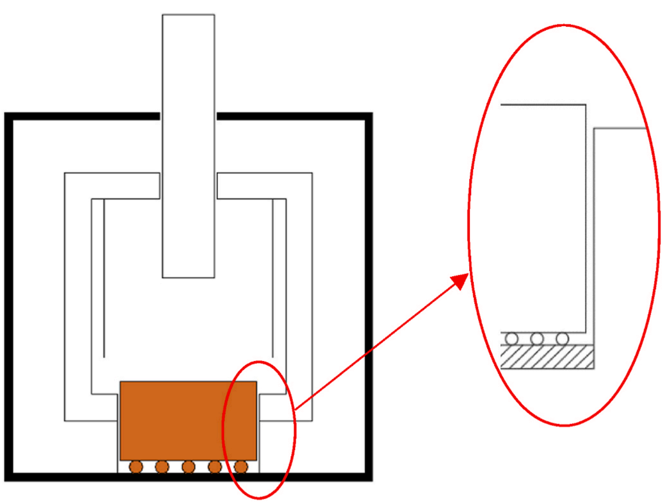

Fig. 4. Modified furnace setup with rollers beneath the lower sample support.

pressure (p) by applying factors between the maximum load, p and q (Table 2), which were determined from linear elastic finite-element simulations. The symmetrical halves of the two sample geometries G1 and G2 were then simulated. A linear 8 node element type C3D8 with an element size of 1 mm was used for meshing [16]. In the simulation, a vertical displacement of 1 mm is applied to the sample. The Young's modulus of the coked MgO–C refractory, which is 4.5 GPa at room temperature was applied for the simulation. However, it should be noted that the Young's modulus does not affect the relation between the maximum load and p_{G1}, q_{G1}, p_{G2}, q_{G2}.

Fig. 2 shows the designated shear volumes of G1 and G2 sample geometries. The mean von Mises stress q and mean hydrostatic pressure p are extracted from this volume. The factors fp and fq for both G1 and G2 were obtained by dividing their respective mean stresses with the reaction forces as shown in Table 2.

The failure points for G1 (p_{G1}/q_{G1}) and G2 (p_{G2}/p_{G2}) are plotted in a p-q diagram (Fig. 1b). With a Drucker-Prager failure line, the cohesion d is represented by the intersection between the failure line with q-axis. As for the friction angle β, it is represented by the angle between the failure line and p-axis. Cohesion d and friction angle β were calculated using equations (4) and (5):

$$d = q_{G2} - p_{G2}\frac{q_{G2} - q_{G1}}{p_{G2} - p_{G1}} \tag{4}$$

$$tan\,\beta = \frac{q_{G2} - q_{G1}}{p_{G1} - p_{G2}} \tag{5}$$

where $q_{G1,G2}$ and $p_{G1,G2}$ are the von Mises stresses and hydrostatic pressures of the respective geometries.

3. Testing setup

A series of tests were performed at room temperature to determine a suitable setup for the subsequent tests at elevated temperatures. These tests focused on three aspects: (1) the influence of rollers beneath the supporting plate of the sample, (2) the sample carrier to achieve reducing conditions for tests at elevated temperatures and (3) to determine possible influences on the sample preparation. For each aspect, three samples of each geometry, 60° and 80° were tested.

First, the influence of the sample restraint from restricted bottom and top pressure plate movements was investigated. Two sets of as-delivered samples were tested without (Fig. 3a) and with (Fig. 3b) rollers beneath the supporting plate. The average of the maximum force for each sample geometry was calculated and presented in Table 3. The two geometries, G1 and G2 showed different results with respect to the influence of the restraint. The 60° notch sample was not significantly affected by the sample restraint, displaying similar mean maximum forces.

For the 80° notch geometry, where the notch intersects the top and bottom surfaces, maximum force required to fracture the sample with rollers and supporting plate is 10% lower relative to that of sample without rollers and supporting plate. Due to the influence of rollers and

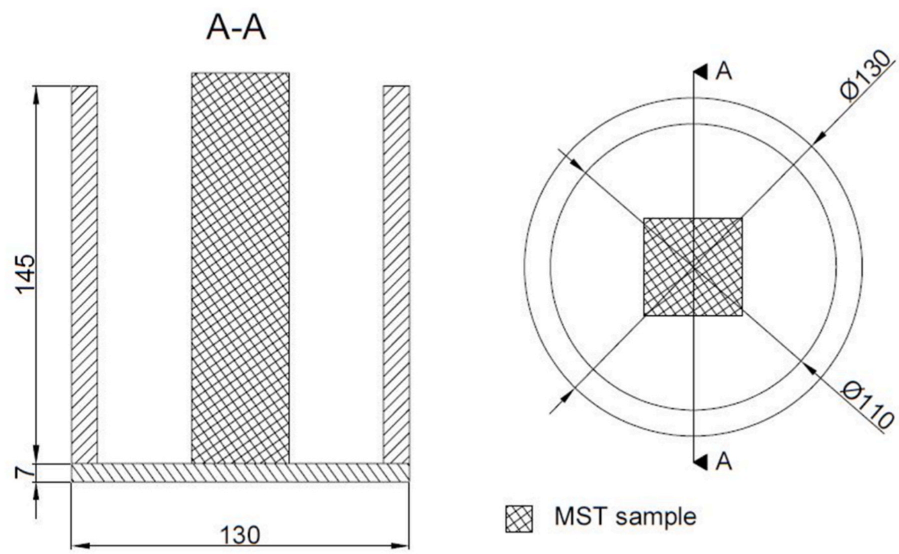

Fig. 5. Sample carrier for testing at elevated temperatures under reducing conditions.

Table 4
Average maximum force of as-delivered samples embedded in coke breeze in the developed sample carrier at room temperature.

	60°-notch samples	80°-notch samples
	force [kN]	force [kN]
MW	24.04	20.29
SD	0.97	0.62

Table 5
Room temperature results of BCS and SCS test series.

	BCS		SCS	
	60°-notch samples	80°-notch samples	60°-notch samples	80°-notch samples
	force [kN]	force [kN]	force [kN]	force [kN]
MW	9.15	5.64	10.5	6.13
SD	0.32	0.16	0.18	0.31

supporting plate on the maximum force, a setup with a plate and rollers beneath the sample was applied for subsequent tests.

The furnace setup was adapted according to previous room temperature results. As depicted in Fig. 4, steel rollers with a diameter of 5 mm, in contact with the water-cooled furnace shell, were added beneath the lower support, which allow movement of the sample support.

To minimise oxidation and bond loss, tests for carbon-containing refractories in the furnace are carried out in reducing conditions at elevated temperatures. A setup that is similar to the tensile and compressive creep testing of carbon-containing refractories presented in Ref. [5] was applied. The MST sample was placed inside the sample carrier and embedded in coke breeze (Fig. 5).

The results could be affected by to the coke breeze surrounding and in direct contact with the MST sample in the carrier. Therefore, a comparison of the mean maximum forces was made between an as-delivered MST sample embedded in coke breeze and another without embedding. As presented in Table 3 (results with plate) and 4, no significant differences were observed between the maximum force of samples with and without embedding in coke breeze. Furthermore, visual inspection of the fracture surfaces also revealed no significant differences between the samples.

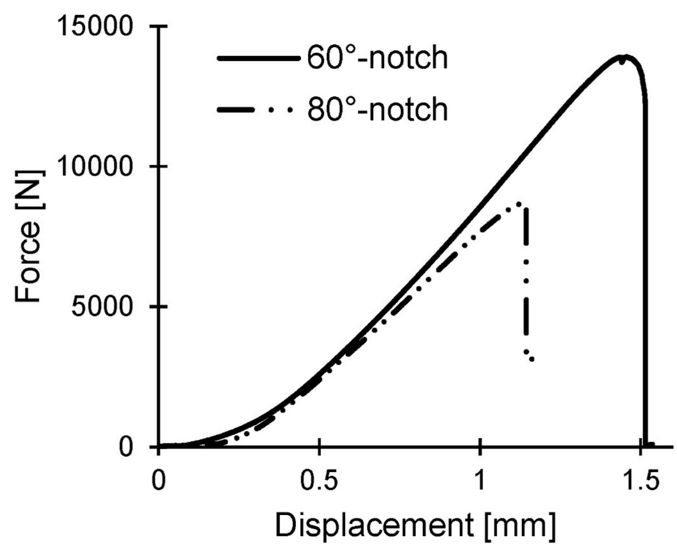

Fig. 6. Exemplary load displacement diagrams of the coked material tested at 400°.

4. Experimental procedure

The setup for testing carbon-containing refractories at elevated temperatures was done based on the preliminary tests, which led to the adapted furnace setup with rollers beneath the lower sample support. To minimise the oxidation of carbon during testing, the samples were embedded in coke breeze. The selected MgO–C refractory was tested in as-delivered and coked state. Coking was performed on the brick at 1000 °C for 5 h under reducing conditions. Temperatures of 400 °C, 800 °C, 1200 °C and 1500 °C were chosen for the elevated temperature testing. Three samples of each 60° and 80°-notch geometry were tested at each temperature.

The testing procedure at elevated temperatures was identical for the as-delivered and coked samples. A sample was placed in the centre of the sample carrier (Fig. 5) while the remaining volume was filled with coke breeze, which itself is not compacted further. The prepared sample carrier was placed in the furnace on the base plate supported by rollers (Fig. 4) and the ceramic piston extension was positioned directly above the sample. The furnace was heated at a rate of 5 K/min until the testing

Table 6
Cohesion d and friction angle β of as-delivered and coked MgO–C refractory material at room- and elevated temperatures.

Temperature [°C]	as-delivered				coked			
	Average force [kN]		d [MPa]	β [°]	Average force [kN]		d [MPa]	β [°]
	60°	*80°*			60°	80°		
25	24.4	20.3	12.1	63.4	10.5	6.1	2.1	70.3
400	21.1	17.4	10.3	63.8	14.8	8.9	3.2	70.1
800	17.9	14.8	8.8	63.5	16.0	9.4	3.3	70.3
1200	16.8	13.9	8.4	63.4	14.8	11.2	5.5	66.8
1500	13.9	11.6	7.0	63.2	9.7	8.3	3.9	66.1

temperature is achieved. A 1 h dwell time was set to ensure thermal homogenisation prior to the test. The sample was loaded consistently at 5 mm/min until fracturing occurred and the load-displacement diagram was recorded. After the fracture, a cooling rate of 5 K/min was applied to cool the samples to room temperature.

5. Results and discussion

The influence of coking on the material parameters at different stages of the sample preparation was studied at room temperature. For the first series of MST samples, the MgO–C brick was coked and followed by cutting (brick-coked samples, BCS). In the second group, MST samples were cut out of as-delivered MgO–C bricks prior to coking (sample-coked samples, SCS).

The results of the mean maximum forces for the BCS and SCS are shown in Table 5. The average maximum force of both MST geometries (60°/80°-notch angle) of the coked samples was significantly lower than that of the as-delivered samples (see also Tables 3 and 4). The differences between the coked samples, BCS and SCS, were 14% and 8% for the 60° and 80°-notch respectively, with the BCS series exhibiting lower absolute values. Conversely, a negligible difference in the friction angle and cohesion was observed between the two groups of samples (BCS: cohesion $d = 2.11$ MPa, friction angle $\beta = 70.3°$, SCS: cohesion $d = 2.06$ MPa, friction angle $\beta = 69.9°$).

Two selected load–displacement curves obtained for the coked material at 400 °C are plotted in Fig. 6. Regardless of the temperature, the 60°-notch samples withstood higher maximum loads than the 80°-notch samples. Furthermore, a higher maximum force was required for as-delivered samples at the same test temperature than for coked samples (see Table 6).

Table 6 presented the average force, d and β values of the coked and as-delivered material for both geometries. Sample pre-treatment is highly influential to the material behaviour at elevated temperatures, which is similar to those at room temperature. A weight loss of 0.5–2.0% typically occurred after the sample testing and the loss increased with temperature. The as-delivered samples exhibited the highest weight loss among the samples. Overall, the maximum force of the materials is temperature-dependent and lower for the coked material. With increasing temperature, the maximum force of coked materials generally increases while that of as-delivered samples exhibited a reverse trend, regardless of the sample geometry. To be precise, the maximum force of coked 60° geometry samples increased up to 800 °C, and decreased above. A similar behaviour is observed for the coked 80° geometry samples in 80° geometry whereby the maximum force increased up to 1200 °C and decreased beyond this temperature.

The cohesion d constantly decreased from 12.1 to 7.0 MPa between the temperature range of 25–1500 °C for the as-delivered samples while the friction angle β remained nearly constant (63.5° ± 0.3°). As for the coked material, the cohesion increased with temperature up to 1200 °C from 2.1 to 5.5 MPa and dropped to 3.9 MPa as the temperature was further increased to 1500 °C. The friction angle remained nearly constant at 70.2° ± 0.2° up to 800 °C and it decreased to 66.4° ± 0.4° at temperatures of 1200 °C and beyond. The applied coking procedure at 1000 °C prior to testing may be used to elucidate the change in results of the coked samples in the temperature range between 800 and 1200 °C. These samples were heated to 1000 °C before and the material undergoes a second heating cycle at temperatures below 1000 °C. Friction angles in a similar range as determined in this work were reported for fresh concrete [17] as well as for other refractory materials [10,18,19].

6. Conclusions

An improved testing setup was introduced to perform MST on carbon containing refractories. This setup allows the determination of friction angle and cohesion from uniaxial loading up to 1500 °C under reducing conditions. In this study, the carbon-containing refractory material was embedded in coke breeze to minimise the occurrence of oxidation during testing at elevated temperatures. Moreover, the samples were supported by a plate resting on rollers to minimise the lateral restrictions.

MST was performed on a resin-bonded magnesia carbon refractory in as-delivered and coked state. Cohesion and friction angle were evaluated at room temperature up to 1500 °C. There are distinct differences between the material parameters obtained for as-delivered and coked material. Particularly, the coked samples exhibit significantly lower cohesion and larger friction angle than the as-delivered samples.

The results may be applied to the simulation of thermomechanical behaviour of refractory linings in service.

Declaration of competing interest

The authors declare that they have no known competing financial interests or personal relationships that could have appeared to influence the work reported in this paper.

Acknowledgment

The authors gratefully acknowledge the funding support of K1-MET GmbH, metallurgical competence center. The research programme of the K1-MET competence center is supported by COMET (Competence Center for Excellent Technologies), the Austrian programme for competence centers. COMET is funded by the Federal Ministry for Climate Action, Environment, Energy, Mobility, Innovation and Technology, the Federal Ministry for Labour and Economy, the Federal States of Upper Austria, Tyrol and Styria as well as the Styrian Business Promotion Agency (SFG) and the Standortagentur Tyrol. Furthermore, Upper Austrian Research GmbH continuously supports K1-MET. Beside the public funding from COMET, this research project is partially financed by the scientific partner Montanuniversitaet Leoben and the industrial partners RHI Magnesita GmbH, voestalpine Böhler Edelstahl GmbH and voestalpine Stahl GmbH.

References

[1] Charles Schacht, Refractories Handbook, first ed., CRC Press, 2004 https://doi.org/10.1201/9780203026328.
[2] D. Gruber, H. Harmuth, Thermomechanical behavior of steel ladle linings and the influence of insulations, steel research int 85 (4) (2014) 512–518, https://doi.org/10.1002/srin201300129.

[3] D. Gruber, K. Andreev, H. Harmuth, FEM simulation of the thermomechanical behaviour of the refractory lining of a blast furnace, J. Mater. Process. Technol. 155–156 (2004) 1539–1543, https://doi.org/10.1016/j.jmatprotec.2004.04.249.

[4] S. Jin, D. Gruber, H. Harmuth, R. Rössler, Thermomechanical failure modeling and investigation into lining optimization for a Ruhrstahl Heraeus snorkel, Eng. Fail. Anal. 62 (2016) 254–262, https://doi.org/10.1016/j-engfailanal.2016.01.014.

[5] M. Stückelschweiger, D. Gruber, S. Jin, H. Harmuth, Creep testing of carbon containing refractories under reducing conditions, Ceram. Int. 45 (8) (2019) 6, https://doi.org/10.1016/j.ceramint.2019.02.013.

[6] Gruber Stückelschweiger, Harmuth Jin, Wedge-splitting test on carbon-containing refractories at high temperatures, Appl. Sci. 9 (16) (2019) 3249, https://doi.org/10.3390/app9163249.

[7] D.C. Drucker, W. Prager, Soil mechanics and plastic analysis or limit design, Q. Appl. Math. 10 (2) (1952) 157–165, https://doi.org/10.1090/qam/48291.

[8] American Society for Testing and Materials ASTM, Standard Test Method for Triaxial Compressive Strength of Undrained Rock Core Samples without Pore Pressure Measurements, 1996. D2664-95a.

[9] J.H. Dieterich, Modeling of rock friction: 1. Experimental results and constitutive equations, J. Geophys. Res. 84 (B5) (1979) 2161–2168, https://doi.org/10.1029/jB084iB05p02161.

[10] Emilie Dahlem, Dietmar Gruber, Thomas Auer, Harald Harmuth, Marc Huger, Thierry Chotard, New methode to determine the cohesion and the friction angle of refractory materials at room temperature and at elevated temperature, in: Proceedings of the 49th Conference of Metallurgists, Advances in Refractories V, 2010, pp. 497–504.

[11] Deutsche Gesellschaft Feuerfest- und Schornsteinbau, Refractory Engineering: Materials - Design - Construction, 2nd revised and updated edition, Vulkan-Verlag GmbH, 2005. ISBN 3-8027-3155-7.

[12] G. Routschka, Taschenbuch Feuerfeste Werkstoffe: Aufbau - Eigenschaften - Prüfung, Vulkan Verlag, Essen, 2007. ISBN 978-3-8027-3157-0.

[13] A.P. Luz, T.M. Souza, C. Pagliosa, M.A.M. Brito, V.C. Pandolfelli, In situ hot elastic modulus evolution of MgO–C refractories containing Al, Si or Al–Mg antioxidants, Ceram. Int. 42 (8) (2016) 9836–9843, https://doi.org/10.1016/j.ceramint.2016.03.080.

[14] H. Baudson, F. Debucquoy, M. Huger, C. Gault, M. Rigaud, Ultrasonic measurement of Young's modulus MgO/C refractories at high temperature, J. Eur. Ceram. Soc. 19 (10) (1999) 1895–1901, https://doi.org/10.1016/50955-2219(98)00268-4.

[15] F. Gong, S. Luo, G. Lin, X. Li, Evaluation of shear strength parameters of rocks by preset angle shear, direct shear and triaxial compression tests, Rock Mech. Rock Eng. 53 (5) (2020) 2505–2519, https://doi.org/10.1007/s00603-020-02050-1.

[16] ABAQUS, Standard User's Manual, Dassault Systèmes Simulia Corp, Providence, RI, 2019.

[17] Q. Yang, Y. Sun, X. Peng, Experimental study on mechanical properties of concrete at super-early age, Materials 15 (21) (2022) 7582, https://doi.org/10.3390/ma15217582.

[18] S. Samadi, S. Jin, D. Gruber, H. Harmuth, Thermomechanical finite element modeling of steel ladle containing alumina spinel refractory lining, Finite Elem. Anal. Des. 206 (2022), 103762, https://doi.org/10.1016/j.finel.2022.103762.

[19] Emilie Dahlem, Characterisation of Refractory Failure under Combined Hydrostatic and Shear Loading at Elevated Temperatures, Dissertation, 2011.